drones

MDPI

Article

Post-Disaster Emergency Communications Enhanced by Drones and Non-Orthogonal Multiple Access: Three-Dimensional Deployment Optimization and Spectrum Allocation

Linyang Li [1,2], Lijun Zhu [1,*], Fanghui Huang [1,3], Dawei Wang [3], Xin Li [3], Tong Wu [1] and Yixin He [1,2,*]

[1] College of Information Science and Engineering, Jiaxing University, Jiaxing 314001, China; linyangli@zjxu.edu.cn (L.L.); huangfanghui@mail.nwpu.edu.cn (F.H.); wutongjx@zjxu.edu.cn (T.W.)
[2] Jiaxing Key Laboratory of Smart Transportations, Jiaxing 314001, China
[3] School of Electronics and Information, Northwestern Polytechnical University, Xi'an 710072, China; wangdw@nwpu.edu.cn (D.W.); xinli@nwpu.edu.cn (X.L.)
* Correspondence: z5l5j5@zjxu.edu.cn (L.Z.); yixinhe@zjxu.edu.cn (Y.H.)

Abstract: Integrating the relaying drone and non-orthogonal multiple access (NOMA) technique into post-disaster emergency communications (PDEComs) is a promising way to accomplish efficient network recovery. Motivated by the above, by optimizing the drone three-dimensional (3D) deployment optimization and spectrum allocation, this paper investigates a quality of service (QoS)-driven sum rate maximization problem for drone-and-NOMA-enhanced PDEComs that aims to improve the data rate of cell edge users (CEUs). Due to the non-deterministic polynomial (NP)-hard characteristics, we first decouple the formulated problem. Next, we obtain the optimal 3D deployment with the aid of a long short-term memory (LSTM)-based recurrent neural network (RNN). Then, we transform the spectrum allocation problem into an optimal matching issue, based on which the Hungarian algorithm is employed to solve it. Finally, the simulation results show that the presented scheme has a significant performance improvement in the sum rate compared with the state-of-the-art works and benchmark scheme. For instance, by adopting the NOMA technique, the sum rate can be increased by 9.72% and the needs of CEUs can be satisfied by enabling the relaying drone. Additionally, the convergence, complexity, and performance gap caused by iterative optimization are discussed and analyzed.

Keywords: drone; non-orthogonal multiple access (NOMA); post-disaster emergency communications (PDEComs); sum rate maximization

Citation: Li, L.; Zhu, L.; Huang, F.; Wang, D.; Li, X.; Wu, T.; He, Y. Post-Disaster Emergency Communications Enhanced by Drones and Non-Orthogonal Multiple Access: Three-Dimensional Deployment Optimization and Spectrum Allocation. *Drones* **2024**, *8*, 63. https://dx.doi.org/10.3390/drones8020063

Academic Editor: Carlos Tavares Calafate

Received: 8 January 2024
Revised: 7 February 2024
Accepted: 9 February 2024
Published: 13 February 2024

1. Introduction

Drones play a crucial role in post-disaster emergency communications (PDEComs), particularly showcasing their advantage as relays [1]. In times of crisis, drones can be rapidly deployed, serving as mobile communication relays to bridge gaps in coverage or areas where ground-based stations are compromised. An illustrative example of this occurred during the 2017 earthquake in Mexico, where ground communication infrastructure was severely damaged. Relaying drones equipped with communication devices were deployed to fly over the affected areas, successfully establishing reliable transmission links. Therefore, the flexible and efficient application of drones in PDEComs has rendered them irreplaceable, elevating rescue efficiency and emergency response capabilities [2].

As relay devices, drones can rapidly establish communication networks. In PDEComs, ground infrastructure may be damaged and traditional communication networks limited. Drones can quickly deploy over affected areas, connecting damaged ground communication equipment through their own communication devices, forming a temporary communication relay station, achieving flexible and efficient communication [3–5]. Moreover, drones can provide extensive coverage in post-disaster environments. Due

to their ability to fly over complex terrain and obstacles, drones can quickly reach different locations in the disaster-stricken area, providing comprehensive coverage for the construction of communication networks [6]. This high maneuverability makes drones an ideal choice for rapidly responding to disasters, effectively overcoming the limitations of ground equipment. Furthermore, drones are typically equipped with advanced sensors and communication technologies, allowing them to collect real-time environmental information and transmit it to command centers. This provides real-time and accurate data support for post-disaster rescue efforts, helping command centers better understand the situation, allocate resources, and formulate rescue plans [7–10]. The high maneuverability and multifunctionality of drones enable them to adapt to various emergency communication needs, improving the efficiency and success rate of post-disaster rescue. In conclusion, drones serve as flexible and efficient relays in PDEComs. With advantages such as rapid network deployment, extensive coverage, and real-time information collection, drones provide powerful support for post-disaster rescue, becoming essential tools in disaster response and emergency communication.

However, the use of the conventional orthogonal multiple access (OMA) technique comes with certain disadvantages. Facing the considered challenges, introducing the non-orthogonal multiple access (NOMA) technique brings a range of functions and advantages [11–13].

- First, the drawback of OMA lies in its relatively low spectrum utilization efficiency. The allocation of orthogonal subcarriers to users in OMA results in spectrum resource wastage, especially when the number of users is low or unevenly distributed. NOMA, on the other hand, allows multiple users to share the same frequency resource on the same subcarrier in a non-orthogonal manner, improving spectrum utilization efficiency, especially in scenarios with an uncertain and uneven distribution of users in PDEComs.
- Second, NOMA exhibits advantages such as higher system throughput and lower channel latency. In OMA, the requirement for orthogonality between subcarriers imposes limitations on the system throughput. NOMA, by allowing multiple users to transmit simultaneously on the same subcarrier, enhances the overall system throughput. Furthermore, NOMA manages interference among users through non-orthogonal means, reducing channel latency and improving communication quality.
- Finally, the introduction of NOMA also serves to increase the connection density and flexibility of emergency communication networks. Due to NOMA allowing multiple users to share the same frequency resource, the emergency communication network can accommodate more user connections, adapting to significant network load fluctuations in PDEComs. Additionally, NOMA exhibits strong flexibility, allowing dynamic resource allocation based on user demands, achieving more flexible and efficient communication.

In this context, the optimization of spectrum resource allocation becomes imperative. Through the rational adjustment of parameters and algorithms in NOMA, it is possible to better meet the communication needs of different disaster-affected users, enhancing the overall performance of emergency communication networks. Spectrum resource allocation optimization also helps prevent spectrum waste, further improving spectrum utilization efficiency. In summary, the introduction of the NOMA technique in PDEComs offers various advantages, including enhanced spectrum utilization efficiency, increased the system throughput, reduced channel latency, and improved connection density and flexibility. Building upon this, optimizing spectrum resource allocation is essential to better meet the complex requirements of PDEComs and enhance the overall performance of emergency communication networks.

Motivated by the above discussions, this paper investigates the application of NOMA and relaying drones in PDEComs. The hovering drone is used as a relay to improve the data rate of CEUs, and the NOMA technique is incorporated into the DF relay protocol to enhance spectrum utilization. Specifically, we formulate a QoS-driven sum rate maximiza-

tion problem by optimizing the drone three-dimensional (3D) deployment optimization and spectrum allocation. To tackle the formulated problem effectively, we first use the long short-term memory (LSTM)-based recurrent neural network (RNN) to solve the optimal 3D deployment with fixed channel assignments. More precisely, by using the RNN, the relaying drone can further adapt to dynamic environmental changes, leading to smarter relay deployments. Then, we reformulate the spectrum allocation problem as an optimal matching issue, based on which the Hungarian algorithm is employed to obtain the optimal spectrum allocation. The complexity of overall algorithmic framework is analyzed theoretically. Finally, the simulation results indicate that the presented scheme is superior to the state-of-the-art works [14–16] and benchmark scheme in terms of the sum rate. Additionally, the convergence, complexity, and performance gap caused by iterative optimization are shown.

2. Related Work

Extensive studies have been carried out to investigate drone-assisted PDEComs [14,17–19]. The work in [17] investigated the sum spectrum efficiency enhancement problem by optimizing the drone service zone selection and user scheduling. In [18,19], the authors optimized the drone deployment with the aim of increasing the data rate of cell edge users (CEUs). Additionally, a drone-assisted urban emergency communication scenario was considered in [14], where a joint altitude and resource allocation scheme was proposed to ensure information forwarding from the disaster area. Currently, in order to make full use of the advantage of drone-assisted PDEComs, combining the NOMA technique with the relaying drone has attracted much attention from researchers [15,16,20,21]. The authors in [15,21] incorporated the NOMA technique with the decode-and-forward (DF) relay protocol to improve the spectrum utilization and transmission performance of PDEComs. Furthermore, by optimally allocating the multi-dimensional resources (e.g., power and time slot scheduling), the energy-efficiency optimization problem was studied in [16,20].

Despite noticeable achievements for data transmissions in PDEComs, the aforementioned works have not exploited the benefits of the combination of drones and NOMA. Several challenging issues remain to be investigated. First, the existing works in [14,17–19] mainly provide relaying services based on the OMA technique for a set of disconnected CEUs. However, employing the NOMA technique can improve the data rate and ensure the connectivity in PDEComs. Second, although the works in [15,16,20,21] adopt the NOMA technique, the advantages of combining the relaying drone with NOMA have yet to be fully exploited. In particular, the authors consider only one-dimensional [21] or two-dimension [15] deployment optimizations. In addition, since using the NOMA technique introduces co-channel interference at CEUs, the spectrum allocation algorithm should be delicately designed in [16,20]. Finally, the above works in [14–21] make an implicit assumption that the basic rate requirement of each CEU can be satisfied. In effect, for the minimum quality of services (QoS) requirement, the fairness of each CEU needs to be guaranteed.

3. System Model and Problem Formulation

As illustrated in Figure 1, we consider the scenario of PDEComs, consisting of a base station (BS), a relaying drone, and M CEUs, denoted as $\mathcal{M} = \{1, \ldots, M\}$. By using the NOMA technique, M CEUs share N frequency channels, denoted as $\mathcal{N} = \{1, \ldots, N\}$. In order to improve the data rate of CEUs, the NOMA technique is integrated into the DF relay protocol. In the NOMA-and-DF-enabled relay protocol, the BS transmits data to the relaying drone in the first time slot (TS). Then, in the second TS, the relaying drone decodes the data and transmits it to M CEUs. Meanwhile, in the second TS, the BS transmits data to M CEUs.

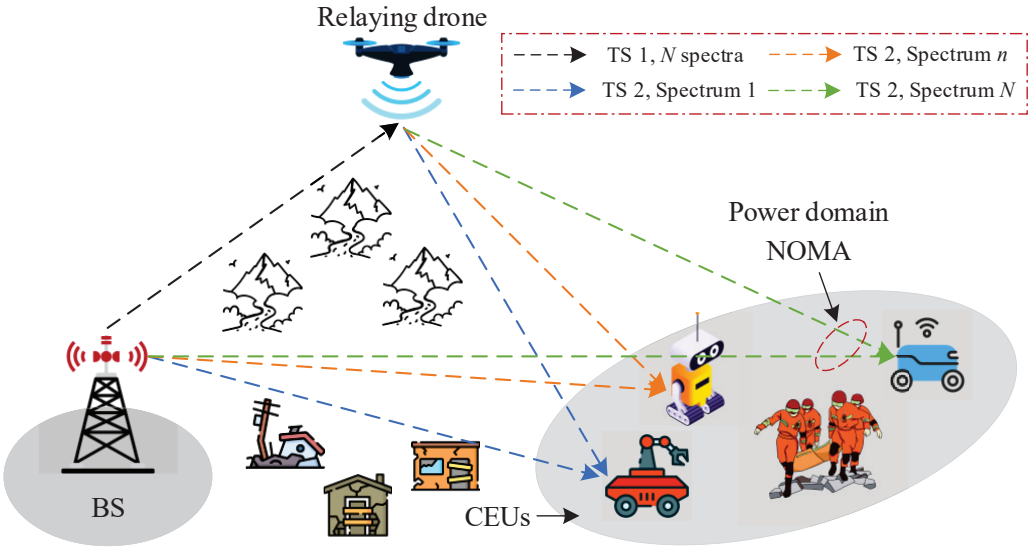

Figure 1. Drone-and-NOMA-enhanced PDEComs.

In emergency situations, ground infrastructures are often damaged, leading to the interruption of line-of-sight (LoS) links. In this situation, the link between the CEU and a remote surviving BS can be regarded as the non-LoS (NLoS) link. By contrast, due to the maneuverability of the drone, the link between it and the CEU is usually the LoS link [21]. Therefore, based on the difference in receiving power, we can use the successive interference cancellation (SIC) technique to recover desired data. Specifically, the CEU prioritizes decoding the signal from the relaying drone. Then, the CEU decodes the signal from the BS. The NOMA-and-DF-enabled relay protocol takes the advantage of the characteristics of power domain NOMA.

Let $\mathcal{X} = \{x_{m,n} | \forall m \in \mathcal{M}, \forall n \in \mathcal{N}\}$ denote the spectrum allocation policy. If the n-th $(\forall n \in \mathcal{N})$ spectrum is allocated to the m-th $(\forall m \in \mathcal{M})$ CEU, $x_{m,n} = 1$, otherwise $x_{m,n} = 0$. Thus, $x_{m,n} \in \{0, 1\}$. The Cartesian coordinate system is introduced in Figure 1. We define the BS location as the origin, and define as the BS antenna height. Therefore, the 3D coordinates of the BS are $\psi_B = (0, 0, H_B)$. Similarly, the 3D coordinates of the drone are $\psi_U = (x, y, z)$, where x, y, and z are the coordinates of horizontal, longitude, and vertical locations for the relaying drone, respectively. In addition, the 3D coordinates of the m-th CEU are $\psi_m = (x_m, y_m, 0)$, where x_m and y_m are the coordinates of horizontal and longitude locations for the m-th CEU, respectively.

For the m-th CEU, the channel power gains of BS–drone, BS–CEU, and drone–CEU are $G^n_{B,U}$, $G^n_{B,m}$, $G^n_{U,m}$, respectively. We have

$$G^n_{B,U} = |s^n_{B,U}|^2 h_{B,U}, \tag{1}$$

$$G^n_{B,m} = |s^n_{B,m}|^2 h_{B,m}, \tag{2}$$

and

$$G^n_{U,m} = |s^n_{U,m}|^2 h_{U,m}, \tag{3}$$

where $s^n_{B,U}$, $s^n_{B,m}$, and $s^n_{U,m}$ are the small-scale fading components of BS–drone, BS–CEU, and drone–CEU, respectively; $h_{B,U}$, $h_{B,m}$, and $h_{U,m}$ are the large-scale fading components of BS–drone, BS–CEU, and drone–CEU, respectively, depending on the pathloss. As discussed in [2], for the air-to-ground link (i.e., the BS–drone and drone–CEU links), the pathloss can be expressed as $32.44 + 20\lg(d(\text{km})) + 20\lg(f_c[\text{MHz}])$, where $d(\cdot)$ is the Euclidean distance, and f_c is the carrier frequency. Specifically, the used pathloss model is the

free-space pathloss model. Based on the theory of electromagnetic wave propagation in a vacuum, the free-space pathloss model considers signal attenuation in unobstructed environments, providing a simple yet accurate representation [22]. In the air-to-ground link (i.e., the BS–drone and drone–CEU links), the aerial paths are typically open, devoid of atmospheric, architectural, or other obstacles. Therefore, employing the free-space pathloss model allows for a reasonably accurate description of signal decay in the air, offering a reliable reference for communication system design. Meanwhile, the application of the free-space pathloss model helps simplify the modeling process of communication systems and provides estimates of pathloss for different transmission distances and frequencies [23–25]. To sum up, choosing the free-space pathloss model for air-to-ground pathloss modeling not only ensures accurate results in practical scenarios but also simplifies the complexity of system design.

Therefore, for the m-th CEU, its data rate $R_m(X, \psi_U)$ is given by

$$R_m(\mathcal{X}, \psi_U) = \sum_{n=1}^{N} x_{m,n} R_{m,n}^{\mathrm{NOMA}}(\psi_U) \geq R_m^{\mathrm{QoS}}, \tag{4}$$

where R_m^{QoS} is the minimum QoS requirement. In (4), the expression of $R_{m,n}^{\mathrm{NOMA}}$ is

$$\begin{aligned} R_{m,n}^{\mathrm{NOMA}}(\psi_U) &= \log_2\left(1 + \frac{P_B G_{B,m}^n}{\sigma^2}\right) \\ &+ \min\left\{\log_2\left(1+\frac{P_B G_{B,U}^n}{\sigma^2}\right), \log_2\left(1+\frac{P_U G_{U,m}^n}{P_B G_{B,m}^n + \sigma^2}\right)\right\}, \end{aligned} \tag{5}$$

where P_B is the BS transmitting power, P_U is the drone transmitting power, and σ^2 is the noise power. According to (4), the sum rate $R^{\mathrm{sum}}(\mathcal{X}, \psi_U)$ is

$$R_m(\mathcal{X}, \psi_U) = \sum_{m=1}^{M} R_m(\mathcal{X}, \psi_U). \tag{6}$$

As introduced above, the drone 3D deployment $(\mathcal{X})$ and spectrum allocation (ψ_U) can significantly affect the sum rate $R^{\mathrm{sum}}(\mathcal{X}, \psi_U)$. Thus, to fully exploit the advantages of drone-and-NOMA-enhanced PDEComs, it is necessary to jointly optimize $(\mathcal{X})$ and (ψ_U). The QoS-driven sum rate maximization problem can be mathematically formulated as

$$\mathrm{P1}: \max_{\mathcal{X}, \psi_U} R^{\mathrm{sum}}(\mathcal{X}, \psi_U) = \sum_{m=1}^{M} R_m(\mathcal{X}, \psi_U) \tag{7a}$$

$$\text{s.t. } \mathrm{C1}: R_m(\mathcal{X}, \psi_U) \geq R_m^{\mathrm{QoS}}, \forall m \tag{7b}$$

$$\mathrm{C2}: \sum_{n=1}^{N} x_{m,n} = 1, \forall m \tag{7c}$$

$$\mathrm{C3}: \sum_{m=1}^{M} x_{m,n} \leq 1, \forall n \tag{7d}$$

$$\mathrm{C4}: x_{m,n} \in \{0, 1\}, \forall m, n \tag{7e}$$

$$\mathrm{C5}: x_{\min} \leq x \leq x_{\max}, \tag{7f}$$

$$\mathrm{C6}: y_{\min} \leq y \leq y_{\max}, \tag{7g}$$

$$\mathrm{C7}: z_{\min} \leq z \leq z_{\max}, \tag{7h}$$

where $x_{\min}$, $y_{\min}$, and $z_{\min}$ are the minimum horizontal, longitude, and vertical locations for the relaying drone, respectively; $x_{\max}$, $y_{\max}$, and $z_{\max}$ are the maximum horizontal, longitude, and vertical locations for the relaying drone, respectively. In P1, C1 ensures that the minimum QoS requirement for each CEU can be satisfied; C2–C4 together de-

fine the spectrum allocation mechanism; C5–C7 together limit the feasible area for the relaying drone.

Remark 1. *This paper adopts a hovering drone. This is because compared with the continuous flight mode, the hovering mode can save energy and extend the flight time of the drone. Meanwhile, by using hovering mode, the drone can maintain a stable position and reduce the instability of communication signals. Second, for power domain NOMA, optimizing P_B and P_U can further improve $R^{sum}(\mathcal{X}, \psi_U)$. However, based on the semi-physical verification, frequent changes in transmitting power will cause the network disconnection. Finally, in the designed NOMA-and-DF-enabled relay protocol, the signal from the BS to the CEU in the first TS is wasted. Theoretically, we can use the maximum ratio combining technique to improve the TS utilization. Unfortunately, due to the limited decoding capability of CEUs, the complex receiving mechanism will be difficult to execute successfully, especially in post-disaster scenarios where electricity and fuel are in short supply.*

4. QoS-Driven Sum Rate Maximization Scheme

Due to $x_{m,n} \in \{0, 1\}$, P1 is a mixed integer nonlinear programming (MINLP) problem with discrete $(\mathcal{X})$ and continuous (ψ_U) variables. To solve it, iterative optimization is used. The overall algorithmic process is summarized in Algorithm 1, where the graph theory and LSTM-based RNN are adopted. In Algorithm 1, the parameters "num_sample" and "num_spectrum" represent the number of samples and the number of frequency channels, respectively. In addition, the parameter "num_CEU" represents the number of CEUs.

Algorithm 1 QoS-driven sum rate maximization scheme

```
Initialize num_sample, num_CEU, num_spectrum.
for i = 1; i ≤ num_sample; i++ do
    Generate the initial position ψ_{U_i} randomly.
    for j = 1; j ≤ num_CEU; j++ do
        Obtain the position ψ_{m_ij} of the m-th CEU.
        Calculate the cost matrix.
        Use the Hungarian algorithm.
    end for
end for
Train the model by using the LSTM-based RNN.
Use the stochastic gradient descent (SGD) algorithm.
Obtain the optimal (X)* and (ψ_U)*.
Output the sum rate.
```

4.1. Spectrum Allocation

Given (ψ_U), P1 can be reduced to

$$\text{P2}: \max_{\mathcal{X}} \; R^{\text{sum}}(\mathcal{X}) = \sum_{m=1}^{M} R_m(\mathcal{X}) \tag{8a}$$

$$\text{s.t. C1} - \text{C4}. \tag{8b}$$

To solve P2, a set of weight coefficients $\{\omega_{m,n}\}$ is introduced, where

$$\omega_{m,n} = \begin{cases} R_{m,n}^{\text{NOMA}}, & R_{m,n}^{\text{NOMA}} \geq R_m^{\text{QoS}}, \\ \Delta, & R_{m,n}^{\text{NOMA}} < R_m^{\text{QoS}}, \end{cases} \tag{9}$$

where Δ is a very small negative value. Substituting $\omega_{m,n}$ into P2, the spectrum allocation problem can be further simplified as

$$\text{P3}: \max_{\mathcal{X}} \sum_{m=1}^{M} \sum_{n=1}^{N} x_{m,n}\omega_{m,n} \tag{10a}$$

$$\text{s.t. } C2 - C4. \tag{10b}$$

It is observed that C1 has been eliminated. As discussed in [26], P3 can be viewed as an optimal matching issue. The optimal spectrum allocation $(\mathcal{X})^*$ can be obtained using the Hungarian algorithm.

4.2. Deployment Optimization

In Section 4.1, we have randomly generated a large number of position data samples of the drone at different locations, and then obtained the optimal spectrum allocation corresponding to the drone at different locations by using the Hungarian algorithm. Through this process, we can determine the sum rate of all CEUs optimized for spectrum allocation when the drone is in different locations. Next, we use these samples to train an LSTM-based RNN model. Specifically, the application of the RNN in solving the deployment optimization problem is primarily based on their powerful modeling capabilities for sequential data. The RNN can handle variable-length sequences and capture dependencies within the sequence through its recurrent structure, making it highly effective in solving convex optimization problems with continuous variables [27–29]. The RNN can gradually adjust parameters by learning temporal information, approaching the optimal solution in a stepwise manner and demonstrating strong optimization performance in convex optimization problems [30].

In the context of 3D optimization deployment of the relaying drone, there are significant advantages to using the RNN. First, the RNN can effectively capture the temporal dynamics of task requirements (i.e., $R_{\tilde{m}}^{\text{QoS}}$), better simulating real deployment scenarios. Second, the RNN can optimize deployment strategies gradually during training, considering dynamic changes in the environment and task priorities, resulting in more flexible and intelligent deployments. Finally, the end-to-end learning capability of the RNN streamlines the deployment process, reducing the need for human intervention and enhancing the system's ability for autonomous decision-making. In summary, employing the RNN to solve the deployment optimization problem provides advantages in modeling sequential data. This advantage leads to more intelligent and adaptive deployment solutions, improving system performance and efficiency.

4.2.1. LSTM-Based RNN

Figure 2 illustrates the RNN feedback structure, where ψ_U is the input, A is the recurrent unit, h represents the weight of neurons, and ReLU represents the activation function. However, the traditional RNN suffers from the vanishing gradient problem, making it difficult to learn long-term dependencies, especially when the current output is related to a distant time series [31]. To overcome this issue, the LSTM units are introduced, which can improve the internal structure of the repetitive modules in a chain-like structure. Figure 3 illustrates the diagram of an LSTM-based RNN. Specifically, LSTM generates a gradient long path by introducing self-loop, and the weight of self-loop is updated accordingly at each iteration. Additionally, LSTM consists of three thresholds, i.e., the input, output, and forgetting thresholds, enhancing the control over the information flow. In Figure 3, the input threshold i_t determines the unit's state that needs to be updated. The output threshold o_t filters the output based on the unit's state. The forgetting threshold f_t determines which information needs to be discarded from the previous time-step's unit state.

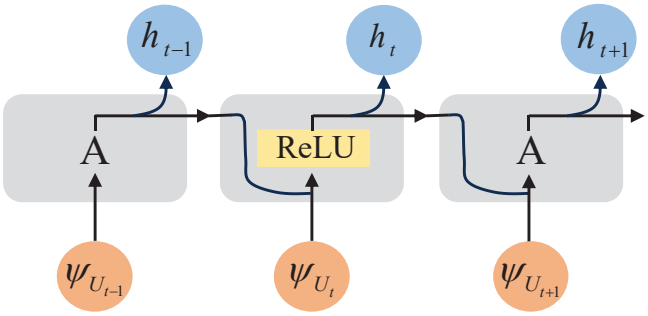

Figure 2. A diagram of an RNN.

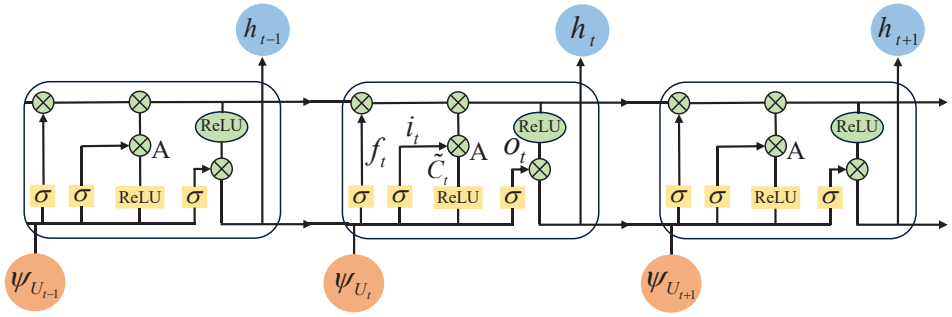

Figure 3. A diagram of an LSTM-based RNN.

The operational principles of LSTM units are

$$f_t = \varepsilon\Big(W_f \cdot [h_{t-1}, \psi_{U_t}] + b_f\Big), \tag{11}$$

$$i_t = \varepsilon(W_i \cdot [h_{t-1}, \psi_{U_t}] + b_i), \tag{12}$$

$$o_t = \varepsilon(W_o \cdot [h_{t-1}, \psi_{U_t}] + b_o), \tag{13}$$

$$\tilde{C}_t = \mathrm{ReLU}(W_C \cdot [h_{t-1}, x_t] + b_C), \tag{14}$$

$$C_t = f_t \cdot C_{t-1} + i_t \cdot \tilde{C}_t, \tag{15}$$

and

$$h_t = o_t \cdot \mathrm{ReLU}(C_t). \tag{16}$$

In (11)–(16), W_f, b_f, W_i, b_i, W_o, and b_o are the weights and biases of three thresholds, respectively; ε is the sigmoid activation function; C_t the state of the RNN unit; and $\tilde{C}_t$ is the state of the LSTM unit.

Figure 4 shows the overall algorithmic flow chart of the proposed deployment optimization algorithm. After the completion of training, we can predict the relationship between the drone 3D deployment and sum rate. In the RNN, the data standardization process is typically performed by subtracting the mean and dividing by the standard deviation. This process aims to eliminate scale differences among the data, ensuring that inputs are within similar ranges. For each time step, the mean of the samples at that time step is taken, subtracted from the samples, and then divided by the standard deviation of the samples at that time step. This ensures that the RNN converges more easily during training, enhancing the stability and generalization capability of the model [32]. Then, in the RNN, the process of data inverse standardization is the inverse operation of standardization. It is executed by multiplying by the standard deviation and adding the mean. During training, to map the model's outputs back to the original scale of the data, the inverse standardization of data is necessary. For each time step, multiply by the standard deviation of the samples at that time step and then add the mean of the samples at that time step. This ensures that the

outputs generated by the RNN can be transformed to the original scale of the data after training, making the model's predictions more meaningful [33].

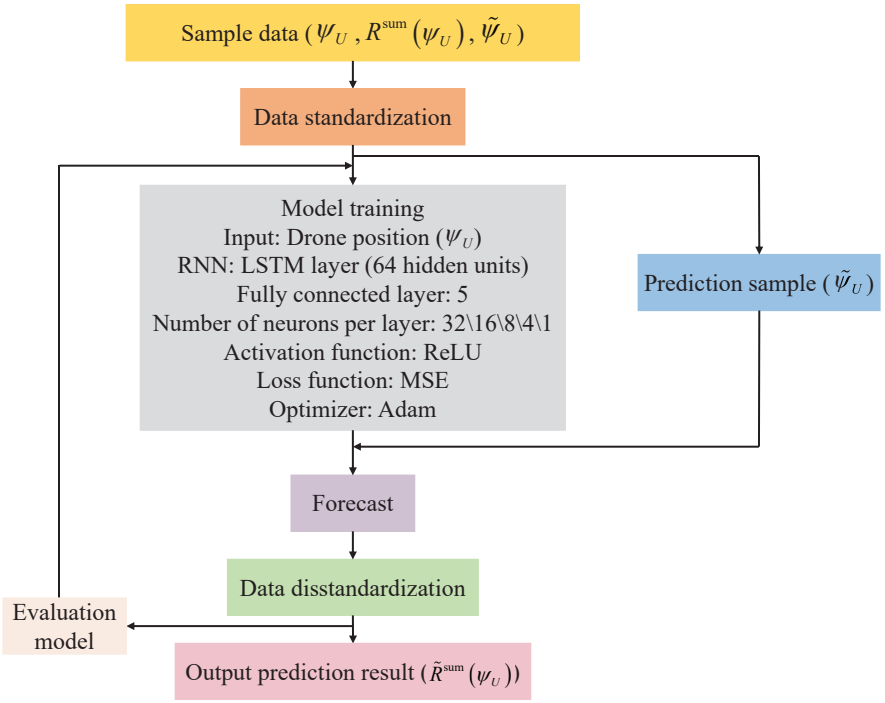

Figure 4. Overall algorithmic flow chart of the proposed deployment optimization algorithm.

4.2.2. SGD Algorithm

During the previous training process, we successfully train a neural network model. This model is designed to take drone 3D deployment as the input and generate the corresponding the sum rate as the output. Given $(\mathcal{X})$, P1 can be reduced to

$$\text{P4}: \max_{\psi_U} \; R^{\text{sum}}(\psi_U) \tag{17a}$$

$$\text{s.t.} \;\; \text{C5} - \text{C7}. \tag{17b}$$

In the proposed scheme, the LSTM-based RNN is employed to learn the relationship between the 3D deployment of the relaying drone and the sum rate. Based on this, the stochastic gradient descent (SGD) algorithm is utilized to guide the updating process by leveraging gradient information to gradually adjust parameters towards the optimal solution. To address this procedure, it is necessary to clarify how to satisfy constraints C5–C7 within the LSTM-based RNN. During the iterative process of the SGD algorithm, the first step involves utilizing a pre-trained neural network model to calculate the sum rate corresponding to the initial location of the drone. Following that, we compute the gradient of the rate with respect to the location, and update the location based on the learning rate and the gradient. After updating the position, a subroutine is invoked to constrain the 3D position of the drone (i.e., to satisfy constraints C5–C7), ensuring that it always remains within the specified range. Subsequently, we recalculate the sum rate. Finally, we need to check that the maximum number of iterations is reached. More precisely, from a program execution point of view, this process includes the following steps. Step 1: We need to check if the horizontal location x is out of bounds. If $x < x_{\min}$, we set $x = x_{\min}$, and if $x > x_{\max}$, we set $x = x_{\max}$. Step 2: We need to check if the longitude location y is out of bounds. If $y < y_{\min}$, we set $y = y_{\min}$, and if $y > y_{\max}$, we set $y = y_{\max}$. Step 3: We need to check if the vertical location z is out of bounds. If $z < z_{\min}$, we set $z = z_{\min}$, and if $z > z_{\max}$, we set $z = z_{\max}$. The mentioned process is repeated until the optimal deployment is achieved. In summary, the drone's position is updated during each iteration of the SGD algorithm,

and position constraints are applied after each update. Through this process, the designed deployment optimization policy ensures that the 3D position of the drone satisfies the constraints C5–C7.

Then, we employ the SGD algorithm to address P4 [34]. For the deployment optimization, we initially set the drone's initial position and normalize the position to satisfy the data input requirements of the aforementioned neural network model. Next, we employ the trained neural network model to predict the sum rate corresponding to the current position. Following this, we calculate the gradient of the rate with respect to the position and update the drone position based on the learning rate and gradient magnitude. Through repeated iterations, we gradually optimize the drone position to maximize the sum rate. Ultimately, when the iteration is over, we output the optimal drone 3D deployment that results in the maximum sum rate. The proposed deployment optimization algorithm is summarized in Algorithm 2. In Algorithm 2, the parameter "learning_rate" represents the learning rate of the SGD algorithm, the parameter "iterations" represents the total number of iterations, the parameter "gradient" represents the partial derivative of rate with respect to the 3D location, which can be regarded as a vector, and the parameter "epsilon" represents the control parameter of learning rate, which can be used to adjust the step size of each gradient update.

Algorithm 2 Deployment optimization algorithm

1: Initialize learning_rate, iterations, gradient, and epsilon.
2: Generate the initial position ψ_U randomly.
3: Standardize the position $\tilde{\psi}_U$.
4: **for** $i = 1$; $i \leq$ iterations; $i++$ **do**
5: Calculate rate $=$ predict(net, $\tilde{\psi}_U$).
6: Renew gradient $= (0, 0, 0)$.
7: **for** $j = 1$; $j \leq 3$; $j++$ **do**
8: Record the temporary variable $\beta = \tilde{\psi}_U$.
9: Calculate the $\beta(j) = \beta(j) +$ epsilon.
10: $R =$ predict(net, β).
11: gradient$(j) = (R -$ rate$)$/epsilon.
12: **end for**
13: Renew the position $\tilde{\psi}_U = \tilde{\psi}_U +$ learning_rate $*$ gradient.
14: rate $=$ predict(net, $\tilde{\psi}_U$).
15: **end for**
16: Denormalized $\tilde{\psi}_{\mathrm{U}}$.
17: Output the optimal spatial position of the drone.

4.3. Complexity Analysis

In this section, we analyze the time complexity of iterative optimization. In Section 4.1, since the time complexity is determined by the Hungarian algorithm, its time complexity is $O(\text{num\_CEU} \times \text{num\_spectrum})$. In Section 4.2.1, the time complexity depends on the size and training options of the LSTM-based RNN model. Thus, its time complexity is $O\left(\text{num\_parameter}(1 + \text{epoch} \times \text{num\_sample})\right)$, where num_parameter is the number of parameters, and epoch is the maximum number of training runs. In Section 4.2.2, since the time complexity of Algorithm 2 is mainly dominated by steps 4 and 7, its time complexity is $O(\text{num\_CEU} \times \text{num\_spectrum}) + O(\text{num\_parameter} \times (1 + \text{epoch} \times \text{num\_sample})) + O(3 \times \text{iterations})$.

5. Simulation Results

In this section, we evaluate the performance of the presented QoS-driven sum rate maximization scheme via simulations. We compare it with the state-of-the-art works and benchmark scheme. The state-of-the-art works are Hu et al.'s scheme [14], He et al.'s scheme [15], and Mirbolouk et al.'s scheme [16]. In the benchmark scheme, the drone

communicates directly with M CEUs. According to [15,21,35], the major simulation parameters are listed as follows, i.e., $M = [0, 30]$, $N = 50$, $H_{\mathrm{B}} = 100$ m, $x_{\max} = y_{\max} = 1000$ m, $x_{\min} = y_{\min} = 20$ m, $z_{\min} = 3$ m, $z_{\max} = 300$ m, $\sigma^2 = -174$ dBm/Hz, $P_B = 4$ Watt, $P_U = 0.5$ Watt, $f_{\mathrm{c}} = 3.5$ GHz, and $R_m^{\mathrm{QoS}} = 1$ bps/Hz. Additionally, the drone coverage radius is 100 m.

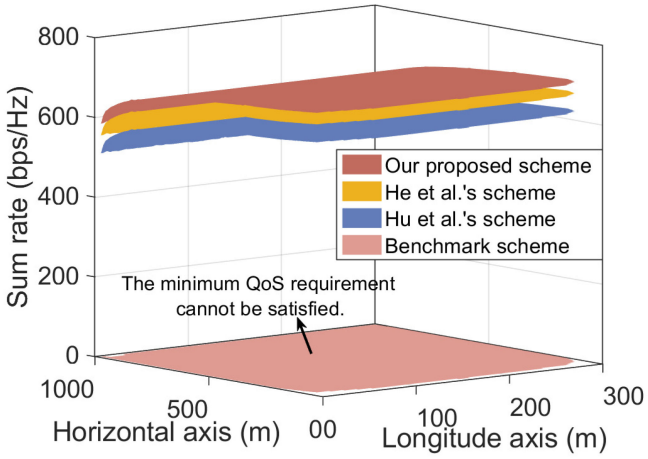

(**a**) The sum rate versus the drone position ($M = 9$ and $N = 50$)

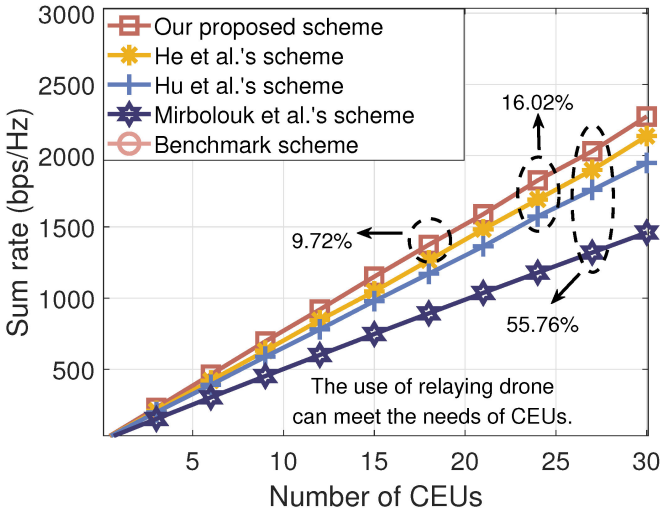

(**b**) The sum rate versus the number of CEUs ($N = 50$)

Figure 5. Performance evaluation [14–16].

Figure 5a plots the sum rate versus the drone position. We can find that the performance of our proposed scheme using the NOMA-and-DF-enabled relay protocol is better than that using the OMA-and-DF-enabled relay protocol (i.e., Hu et al.'s scheme). This confirms the effectiveness of integrating NOMA into the DF relay protocol. Additionally, by observing the benchmark scheme, we know that if the relaying drone is not used in PDEComs, the minimum QoS requirement of CEUs may not be satisfied. Figure 5b shows the sum rate versus the number of CEUs. It can be observed that the sum rate increases with the number of CEUs in drone-and-NOMA-enhanced PDEComs. In particular, our proposed scheme has the highest sum rate regardless of the number of CEUs. Compared to He et al.'s scheme, Hu et al.'s scheme, and Mirbolouk et al.'s scheme, the sum rate can be increased by 9.72%, 16.02%, and 55.76%, respectively.

Figures 6a,b depict the comparison of running time with respect to the number of simulation runs under the different number of CEUs, where the running time is used as

the index of complexity comparison. It is observed that the time complexity of the three schemes is similar. In addition, when M is increased from 15 to 30, there is no significant increase in running time. The above results are very beneficial for CEUs with limited resources in post-disaster scenarios. These simulation results also show the effectiveness of our proposed scheme from another side.

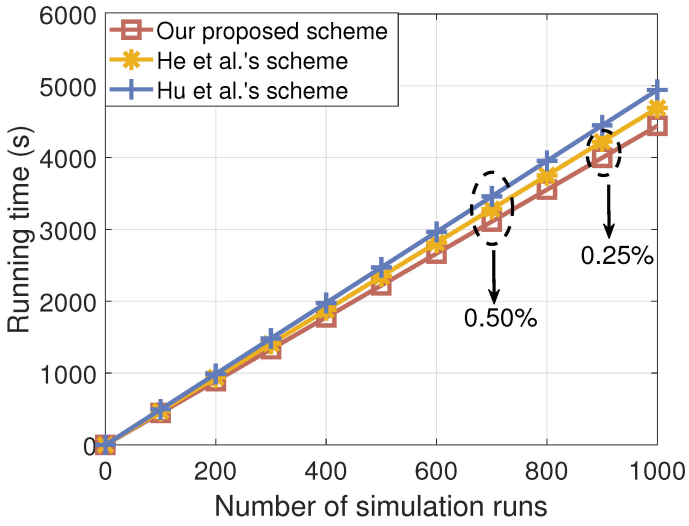

(**a**) $M = 15$

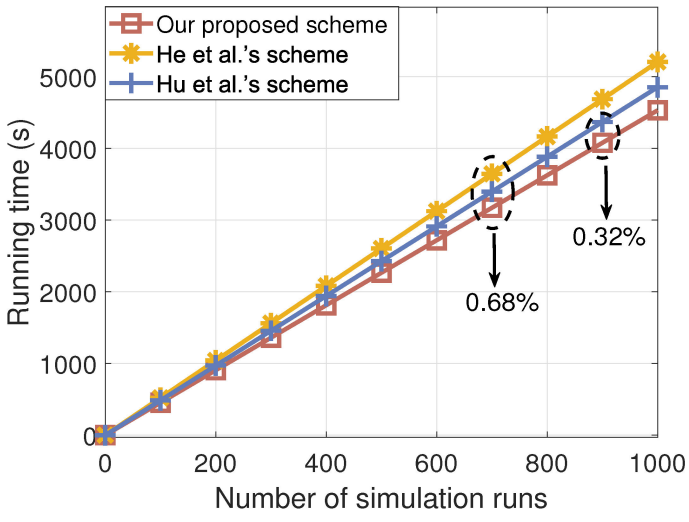

(**b**) $M = 30$

Figure 6. Complexity comparison [14,15].

Figure 7a shows the convergence of our scheme. We can find that our scheme can converge quickly, and the iteration number is about 41. This phenomenon shows that it is efficient to solve P1 by using iterative optimization. Moreover, based on Figure 7b, we investigate the performance gap caused by iterative optimization. In order to obtain the global optimal solution, we use the enumeration scheme. The performance gap is about 1.23%. This is because the design philosophy of decoupling P1 is dependent on the coordinate polling approach. Under this condition, optimality is lost. However, since the performance gap is minimal, it is reasonable and meaningful to apply our scheme to actual PDEComs.

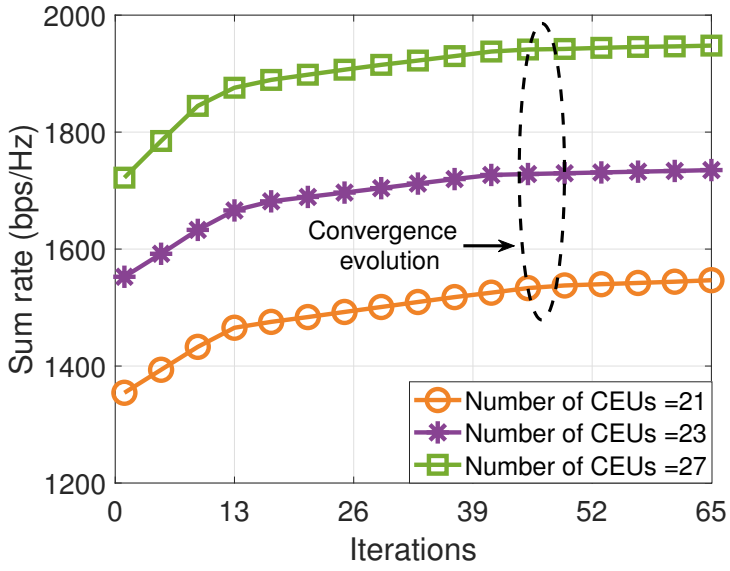

(**a**) Convergence

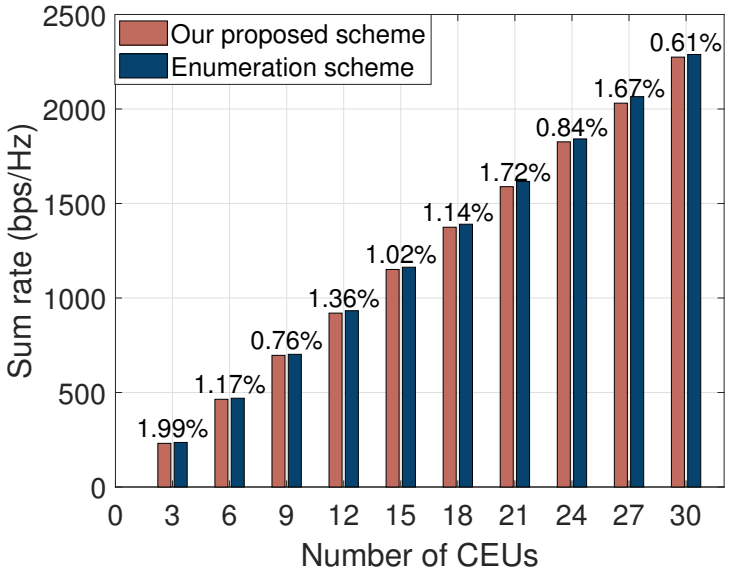

(**b**) Performance gap

Figure 7. Performance analysis.

6. Conclusions

This paper proposed the NOMA-and-DF-enabled relay protocol for PDEComs, and adopted the drone as the relay to improve the data rate of CEUs. On this basis, the QoS-driven sum rate maximization problem was formulated by jointly considering the drone 3D deployment optimization, spectrum allocation, and minimum QoS requirement. To tackle the formulated problem, we adopted the graph theory and LSTM-based RNN, respectively, to deal with the deployment optimization and spectrum allocation. Finally, the simulation results verified that the proposed scheme outperformed the state-of-the-art works and benchmark scheme in terms of the sum rate. Moreover, we analyzed the complexity from both theoretical and simulation aspects and studied the convergence and performance gap caused by iterative optimization via simulations.

As our future work, we plan to investigate emergency communication scenarios where multiple relaying drones collaborate to further expand the range of services. There are several aspects that deserve further study. (1) Collaborative control and path planning: How to achieve collaborative control among multiple relay drones to ensure effective cooperation

in completing communication tasks. (2) Communication protocols and data transmission: We can develop efficient communication protocols for multiple relaying drones, ensuring reliable data transmission. (3) Emergency communication algorithms and real-time optimization: We can research real-time algorithms for emergency communication to adjust drone task assignments and communication strategies based on real-time requirements and design decision-making algorithms for intelligent and timely responses to rapidly changing conditions in disaster scenarios. (4) Autonomous perception and obstacle avoidance technique: We need to propose obstacle avoidance techniques in complex environments to ensure safe drone operation in post-disaster scenarios and develop autonomous perception systems for multiple relay drones to avoid collisions and enhance aerial safety.

Author Contributions: L.L.: conceptualization, methodology, software, and writing—original draft preparation. L.Z.: conceptualization, resources, writing—review and editing, supervision, and funding acquisition. F.H.: resources, funding acquisition, and writing—review and editing. D.W.: conceptualization, resources, and writing—review and editing. X.L.: formal analysis and writing—review and editing. T.W.: resources, writing—review and editing, and funding acquisition. Y.H.: conceptualization, resources, writing—review and editing, supervision, project administration, and funding acquisition. All authors have read and agreed to the published version of the manuscript.

Funding: This work was supported in part by the Zhejiang Provincial Natural Science Foundation of China under Grant LQ24F010003, in part by the Key Research and Development Program of Zhejiang Province under Grants 2024C04004, 2022C03121 and 2023C01162, in part by the National Natural Science Foundation of China under Grant 62271399, in part by the National Key Research and Development Program of China under Grant 2020YFB1807003, and in part by the Natural Science Basic Research Program of Shaanxi Province under Grant 2021JM-074.

Institutional Review Board Statement: Not applicable.

Informed Consent Statement: Not applicable.

Data Availability Statement: Data are contained within the article.

Conflicts of Interest: The authors declare no conflicts of interest for publishing in this journal.

References

1. Tran, D.-H.; Nguyen, V.-D.; Chatzinotas, S.; Vu, T.X.; Ottersten, B. UAV relay-assisted emergency communications in IoT networks: Resource allocation and trajectory optimization. *IEEE Trans. Wireless Commun.* **2022**, *21*, 1621–1637. [CrossRef]
2. Prasad, N.-L.; Ramkumar, B. 3-D Deployment and Trajectory Planning for Relay Based UAV Assisted Cooperative Communication for Emergency Scenarios Using Dijkstra's Algorithm. *IEEE Trans. Veh. Technol.* **2023**, *72*, 5049-5063. [CrossRef]
3. Xiao, Z.; Han, Z.; Nallanathan, A.; Dobre, O.A.; Clerckx, B.; Choi, J.; He, C.; Tong, W. Antenna array enabled space/air/ground communications and networking for 6G. *IEEE J. Sel. Areas Commun.* **2022**, *40*, 2773–2804. [CrossRef]
4. Schweiger, K.; Preis, L. Urban air mobility: Systematic review of scientific publications and regulations for vertiport design and operation. *Drones* **2022**, *6*, 179. [CrossRef]
5. Alsamhi, S.H.; Shvetsov, A.V.; Kumar, S.; Hassan, J.; Alhartomi, M.A.; Shvetsova, S.V.; Sahal, R.; Hawbani, A. Computing in the sky: A survey on intelligent ubiquitous computing for UAV-assisted 6G networks and industry 4.0/5.0. *Drones* **2022**, *6*, 177. [CrossRef]
6. Aggarwal, S.; Kumar, N.; Tanwar, S. Blockchain-envisioned UAV communication using 6G networks: Open issues, use cases, and future directions. *IEEE Internet Things J.* **2021**, *8*, 5416–5441. [CrossRef]
7. Zhang, J.; Sheng, H.; Chen, Q.; Zhou, H.; Yin, B.; Li, J.; Li, M. A four-dimensional space-time automatic obstacle avoidance trajectory planning method for multi-UAV cooperative formation flight. *Drones* **2022**, *6*, 192. [CrossRef]
8. Khoufi, I.; Laouiti, A.; Adjih, C. A survey of recent extended variants of the traveling salesman and vehicle routing problems for unmanned aerial vehicles. *Drones* **2019**, *3*, 66. [CrossRef]
9. Tang, X.; Chen, F.; Wang, F.; Jia, Z. Disaster-resilient emergency communication with intelligent air-ground cooperation. *IEEE Internet Things J.* **2024**, *11*, 5331–5346. [CrossRef]
10. Chen, R.; Cheng, W.; Ding, Y.; Wang, B. QoS-guaranteed multi-UAV coverage scheme for IoT communications with interference management. *IEEE Internet Things J.* **2024**, *11*, 4116–4126. [CrossRef]
11. Zhou, Y.; Wong, V.W.S.; Schober, R. Dynamic decode-and-forward based cooperative NOMA with spatially random users. *IEEE Trans. Wirel. Commun.* **2018**, *17*, 3340–3356. [CrossRef]
12. He, Y.; Wang, D.; Huang, F.; Zhang, R.; Gu, X.; Pan, J. A V2I and V2V collaboration framework to support emergency communications in ABS-aided Internet of Vehicles. *IEEE Trans. Green Commun. Netw.* **2023**, *7*, 2038–2051. [CrossRef]

13. Wang, J.; Liu, M.; Sun, J.; Gui, G.; Gacanin, H.; Sari, H.; Adachi, F. Multiple unmanned-aerial-vehicles deployment and user pairing for nonorthogonal multiple access schemes. *IEEE Internet Things J.* **2021**, *8*, 1883–1895. [CrossRef]
14. Hu, B.; Wang, L.; Chen, S.; Cui, J.; Chen, L. An uplink throughput optimization scheme for UAV-enabled urban emergency communications. *IEEE Internet Things J.* **2022**, *9*, 4291–4302. [CrossRef]
15. He, Y.; Huang, F.; Wang, D.; Zhang, R.; Gu, X.; Pan, J. NOMA- and MRC-enabled enabled framework in drone-relayed vehicular networks: Height/trajectory optimization and performance analysis. *IEEE Internet Things J.* **2023**, *10*, 22305–22319. [CrossRef]
16. Mirbolouk, S.; Valizadeh, M.; Amirani, M.C.; Ali, S. Relay selection and power allocation for energy efficiency maximization in hybrid satellite-UAV networks with CoMP-NOMA transmission. *IEEE Trans. Veh. Technol.* **2022**, *71*, 5087–5100. [CrossRef]
17. Wang, C.; Deng, D.; Xu, L.; Wang, W. Resource scheduling based on deep reinforcement learning in UAV assisted emergency communication networks. *IEEE Trans. Commun.* **2022**, *70*, 3834–3848. [CrossRef]
18. Yao, Z.; Cheng, W.; Zhang, W.; Zhang, H. Resource allocation for 5G-UAV-based emergency wireless communications. *IEEE J. Sel. Areas Commun.* **2021**, *39*, 3395–3410. [CrossRef]
19. Zhong, X.; Guo, Y.; Li, N.; Chen, Y. Joint optimization of relay deployment channel allocation and relay assignment for UAVs-aided D2D networks. *IEEE/ACM Trans. Netw.* **2020**, *28*, 804–817. [CrossRef]
20. Wang, N.; Li, F.; Chen, D.; Liu, L.; Bao, Z. NOMA-based energy-efficiency optimization for UAV enabled space-air-ground integrated relay networks. *IEEE Trans. Veh. Technol.* **2022**, *71*, 4129–4141. [CrossRef]
21. Zhai, D.; Li, H.; Tang, X.; Zhang, R.; Ding, Z.; Yu, F.R. Height optimization and resource allocation for NOMA enhanced UAV-aided relay networks. *IEEE Trans. Commun.* **2021**, *69*, 962–975. [CrossRef]
22. Wang, K.; Zhang, R.; Wu, L.; Zhong, Z.; He, L.; Liu, J.; Pang, X. Path loss measurement and modeling for low-altitude UAV access channels. In Proceedings of the 2017 IEEE 86th Vehicular Technology Conference (VTC-Fall), Toronto, ON, Canada, 24–27 September 2017; pp. 1–5.
23. Bian, J.; Wang, C.-X.; Liu, Y.; Tian, J.; Qiao, J.; Zheng, X. 3D non-stationary wideband UAV-to-ground MIMO channel models based on aeronautic random mobility model. *IEEE Trans. Veh. Technol.* **2021**, *70*, 11154–11168. [CrossRef]
24. Ge, C.; Zhang, R.; Zhai, D.; Jiang, Y.; Li, B. UAV-correlated MIMO channels: 3-D geometrical-based polarized model and capacity analysis. *IEEE Internet Things J.* **2023**, *10*, 1446–1460. [CrossRef]
25. Liu, Y.; Wang, C.-X.; Chang, H.; He, Y.; Bian, J. A novel non-stationary 6G UAV channel model for maritime communications. *IEEE J. Sel. Areas Commun.* **2021**, *39*, 2992–3005. [CrossRef]
26. Liang, L.; Kim, J.; Jha, S.C.; Sivanesan, K.; Li, G.Y. Spectrum and power allocation for vehicular communications with delayed CSI feedback. *IEEE Wireless Commun. Lett.* **2017**, *6*, 458–461. [CrossRef]
27. Dang, Y.; Karakoc, A.; Norshahida, S.; Jäntti, R. 3D radio map-based GPS spoofing detection and mitigation for cellular-connected UAVs. *IEEE Trans. Mach. Learn. Commun. Netw.* **2023**, *1*, 313–327. [CrossRef]
28. Wang, Q.; Liu, Q.; Xia, R.; Li, G.; Gao, J.; Zhou, H.; Zhao, B. Defect depth determination in laser infrared thermography based on LSTM-RNN. *IEEE Access* **2020**, *8*, 153385–153393. [CrossRef]
29. Shehzad, M.K.; Rose, L.; Assaad, M. RNN-based twin channel predictors for CSI acquisition in UAV-assisted 5G+ networks. In Proceedings of the IEEE Global Communications Conference (GLOBECOM), Madrid, Spain, 7–11 December 2021; pp. 1–6.
30. Jiang, Y.; Nihei, K.; Li, J.; Yoshida, H.; Kanetomo, D. Learning on the fly: An RNN-based online throughput prediction framework for UAV communications. In Proceedings of the IEEE International Conference on Communications Workshops (ICC Workshops), Dublin, Ireland, 7–11 June 2020; pp. 1–7.
31. Shan, D.; Luo, Y.; Zhang, X.; Zhang, C. DRRNets: Dynamic recurrent routing via low-rank regularization in recurrent neural networks. *IEEE Trans. Neural Netw. Learn. Syst.* **2023**, *34*, 2057–2067. [CrossRef]
32. Rama-Maneiro, E.; Vidal, J.C.; Lama, M. Embedding graph convolutional networks in recurrent neural networks for predictive monitoring. *IEEE Trans. Knowl. Data Eng.* **2024**, *36*, 137–151. [CrossRef]
33. Beiran, M.; Spencer-Salmon, C.A.; Rajan, K. A 'programming' framework for recurrent neural networks. *Nat. Mach. Intell.* **2023**, *5*, 570–571. [CrossRef]
34. Boyd, S.; Vandenberghe, L. *Convex Optimization*; Cambridge University Press: Cambridge, UK, 2004.
35. Khawaja, W.; Guvenc, I.; Matolak, D.W.; Fiebig, U.-C.; Schneckenburger, N. A survey of air-to-ground propagation channel modeling for unmanned aerial vehicles. *IEEE Commun. Surv. Tutor.* **2019**, *21*, 2361–2391. [CrossRef]